Theoretical cross sections for H-on-Cs ionic and neutral reactions

R. E. Olson*
Service de Physique Atomique, Centre d'Etudes Nucléaires de Saclay, 91190 Gif-sur-Yvette, France

E. J. Shipsey† and J. C. Browne†
Departments of Physics and Computer Sciences, University of Texas at Austin, Austin, Texas
(Received 4 August 1975)

Potential-energy curves and coupling matrix elements have been calculated for the CsH and CsH^+ systems. The potentials and coupling terms were employed in the coupled equations where the nuclear motion is described classically to obtain the energy dependence of the cross sections for energies 0.1–3.0 keV. The cross sections so obtained were: Q_{+0} for the reaction $H^+ + Cs \rightarrow H + Cs^+$, Q_{+m} for $H^+ + Cs \rightarrow H(2s) + Cs^+$, Q_{-0} for $H^- + Cs^+ \rightarrow H + Cs$, and Q_{0-} for $H(1s) + Cs \rightarrow H^- + Cs^+$. The CsH potential-energy curves were also used to estimate the ionization cross sections $Q_{\text{ion-Cs}}$ for $H^- + Cs \rightarrow H^- + Cs^+ + e$ and $Q_{\text{ion-H}}$ for $H^- + Cs \rightarrow H + Cs + e$, and to yield an upper-limit cross section Q_{m-} for the reaction $H(2s) + Cs \rightarrow H^- + Cs^+$. Semiempirical calculations were employed to obtain the deactivation cross section $Q_{m\ell}$ for $H(2s) + Cs \rightarrow H(2p) + Cs$ where the product $H(2p)$ rapidly radiates to $H(1s)$. At 0.5 keV the theoretical cross sections obtained were $Q_{+0} = 1.2\times10^{-14}$, $Q_{+m} = 5.5\times10^{-15}$, $Q_{-0} = 1.5\times10^{-14}$, $Q_{0-} = 8.2\times10^{-16}$, $Q_{\text{ion-Cs}} = 1.3\times10^{-15}$, $Q_{\text{ion-H}} = 2.9\times10^{-15}$, $Q_{m\ell} = 8.1\times10^{-15}$, and $Q_{m-} \leq 4\times10^{-16}$ cm^2. For the reactions where experimental data is available, the theoretical cross sections are in satisfactory agreement with experiment except for Q_{0-}, where the theoretical values are approximately a factor of 5 larger than the experimental values.

I. INTRODUCTION

There has been considerable interest in recent years on the reactions of hydrogen and cesium neutrals and ions at low to moderate collision energies, $E \lesssim 3$ keV. The practical reason behind this interest arises because the reaction

$$H^+ + Cs \rightarrow H(2s) + Cs^+ + 0.49 \text{ eV} \quad (1)$$

is one of the most efficient ways (largest cross section) for producing beams of metastable $H(2s)$ atoms. The metastable $H(2s)$ atoms can be polarized by selective quenching of hyperfine states in magnetic and electric fields; then, by subsequently colliding the polarized $H(2s)$ with a gas such as Ar or Kr,

$$H(2s) + Ar \rightarrow H^- + Ar^+, \quad (2)$$

it is possible to produce polarized H^- ions. Reactions (1) and (2) are the basis[1,2] for polarized ion sources that are used as injectors for tandem accelerators. Since reaction (1) has its largest cross section[3] at 0.5 keV and because the polarized ion sources are operated under thick-target conditions (multiple collisions), all the reactions of H and Cs ions and neutrals at energies $E \approx 0.5$ keV are of fundamental interest. Reaction (2) has been the topic of a previous study where it was suggested that at 0.5 keV, Kr and not Ar would produce the largest usable beam of H^- ions.[4]

In this study, we have generated potential-energy curves and coupling matrix elements for CsH and CsH^+ and have used them in classical close-coupled calculations to obtain the cross sections for several H-Cs reactions from 0.1 to 3.0 keV. These reactions include (the cross section notation is also given):

$$H^+ + Cs \rightarrow H + Cs^+, \quad Q_{+0}, \quad (3)$$

$$H^+ + Cs \rightarrow H(2s) + Cs^+, \quad Q_{+m}, \quad (4)$$

$$H^- + Cs^+ \rightarrow H + Cs, \quad Q_{-0}, \quad (5)$$

and

$$H(1s) + Cs \rightarrow H^- + Cs^+ + 3.14 \text{ eV}, \quad Q_{0-}. \quad (6)$$

In reaction (3), the unspecified state of the product H means all the possible levels of H that are available for reaction. Also, using the potential curves for CsH and a theoretical technique developed to understand $He(2\,^3S) + He$ differential ionization cross sections,[5] it is possible to estimate the cross sections for the ionization reactions

$$H^- + Cs \rightarrow H^- + Cs^+ + e, \quad Q_{\text{ion-Cs}}, \quad (7)$$

and

$$H^- + Cs \rightarrow H + Cs + e, \quad Q_{\text{ion-H}}. \quad (8)$$

For reactions (7) and (8), the calculations were carried out to 10 keV so that comparison could be made with existing experimental data.[6] The

cross section for the reaction

$$H(2s) + Cs \rightarrow H(2p) + Cs, \quad Q_{m\ell} \qquad (9)$$
$$\downarrow h\nu \rightarrow H(1s)$$

has also been calculated and compared to experimental data[7] by using a semiempirical method described previously.[8] Finally, utilizing the CsH potential curves, it is possible to estimate an upper-limit cross section for the reaction

$$H(2s) + Cs \rightarrow H^- + Cs^+, \quad Q_{m-}. \qquad (10)$$

For reactions (3)–(10), the theoretical cross sections are compared to experimental data when it is possible. The only other theoretical study of a H-Cs reaction is that of Valance and Spiess,[9] who have utilized pseudopotentials to calculate the cross section for reaction (4).

II. DEFINITION OF THE MOLECULAR REPRESENTATION BASIS

The energy range of interest in the collision processes assures that the cross-section behavior will be dominated by the interactions of the molecular wave functions and potential surfaces defined by the initial and final atomic states. Therefore, processes (3)–(6) are modeled in a basis of such molecular states and in terms of transitions between these states. The Hamiltonians used are those of one- or two-electron heteronuclear molecules.

A. $(CsH)^+$ system

The lowest $^2\Sigma$ ($1\,^2\Sigma$) state of the CsH^+ molecular system arises in the separated-atom origin $Cs^+ + H(1s)$. The next set of three $^2\Sigma$ states arises from $Cs(6s) + H^+$ ($2\,^2\Sigma$) and from $Cs^+ + H(n=2)$ ($3,4\,^2\Sigma$). There is also a state of $^2\Pi$ symmetry ($1\,^2\Pi$) arising from the $Cs^+ + H(n=2)$ separated atoms. The next states of possible interest are the $^2\Pi$ ($2\,^2\Pi$) and $^2\Sigma$ ($5\,^2\Sigma$) states originating in the $Cs(6p) + H^+$ separated atoms. The set of states $2, 3, 4\,^2\Sigma$ and $1\,^2\Pi$ are, in the region of internuclear separation dominant in the collision process, very close in energy (~0.02 a.u.) and relatively widely separated (~0.06 a.u.) from the $1\,^1\Sigma$ and $2\,^2\Pi - 5\,^2\Sigma$ states. Thus, the representation of the collision processes (3) and (4) is resolved to the procurement of a molecular wave-function basis and the coupling matrix elements for the $2, 3, 4\,^2\Sigma$ and the $1\,^2\Pi$ states of the CsH^+ molecular ion. The wave functions are approximated by a one-electron model. The orbital basis for the wave functions included extensive provision for representation of polarization since the transition processes primarily take place at large internuclear separations.

The $^2\Sigma$ wave functions were of the form

$$\Psi(^2\Sigma) = C_1 4s_{Cs} + C_2 4p_{0,Cs} + C_3 4d_{0,Cs} + C_4 4f_{0,Cs} + C_5 1s_H + C_6 2s_H + C_7 2p_{0,H} + C_8 3s_H + C_9 3p_{0,H} + C_{10} 3d_{0,H}. \qquad (11)$$

The $^2\Pi$ wave function was of the form

$$\Psi(^2\Pi) = C_1 4p_{+,Cs} + C_2 4d_{+1,Cs} + C_3 4f_{+1,Cs} + C_4 2p_{+,H} + C_5 3p_{+,H} + C_6 3d_{+1,H}. \qquad (12)$$

The orbitals, except for the $2s_H$ which were given hydrogenic form, were Slater-type orbitals. Slater's rules[10] give an effective quantum number of 4.2 for the $n=6$ atomic orbitals of Cs, so $n=4$ was used for the $Cs(n=6)$ orbitals. The orbital exponents of the $4s_{Cs}$ orbital were chosen to reproduce the known Cs $6s$-$6p$ splitting to ensure correct relative placement at large internuclear separations. The 2, 3, and $4\,^2\Sigma$ states were obtained as the second, third, and fourth eigenvectors and eigenvalues resulting from application of the linear variation principle[11] to $\Psi(^2\Sigma)$. The $1\,^2\Pi$ state was obtained as the lowest eigenvector and eigenvalue resulting from application of the linear variation principle to $\Psi(^2\Pi)$. The resulting potential curves are shown in Fig. 1.

B. CsH system

The initial and final states of processes (5) and (6) are an $H(^2S)$ atom, an $H^-(^1S)$ ion, a Cs atom, and a $Cs^+(^1S)$ ion. Only the Cs(6s) and Cs(6p) atomic states need to be included in the molecular representation. The necessary set of molecular states thus becomes the three lowest states of $^1\Sigma$ symmetry ($1, 2, 3, ^1\Sigma$) and the lowest state of $^1\Pi$ symmetry ($1\,^1\Pi$). We herein adopt a one-electron model of the Cs atom states and a bare nucleus of charge +1 for the Cs ion. The necessary set of molecular states can then be represented with a two-electron model. The $^1\Sigma$ wave functions have the form

$$\Psi(^1\Sigma) = C_1 1s_H 4s_{Cs} + C_2 1s_H 4p_{0,Cs} + C_3 1s'_H 1s''_H + C_4 (2p_{0,H})^2 + C_6 2p_{+,H} 2p_{-,H}. \qquad (13)$$

The lowest $^1\Pi$ state is formed from $Cs(6p_+)$, and the approximate wave function has the form

$$\Psi(^1\Pi) = 1s_H 4p_{+,Cs}. \qquad (14)$$

The $4s$ and the $4p$ Slater-type orbitals are used to represent the $Cs(n=6)$ levels just as in the $(CsH)^+$ system. It is readily possible to obtain the correct relative energy splittings in the separated-atom limit. The energy of the H atom is, of course, known exactly. The use of the two-term represen-

tation[12] for the H^- ion yields the correct separated-atom energy for the initial state of (5) to within 0.002 a.u.. The two-orbital exponents of the Cs orbitals were chosen to yield the proper endothermicity for reaction (5) and to yield the correct energy splitting for the Cs $6s - 6p_0 - 6p_+$ separated-atom states. The fine-structure splitting of the Cs $6p_0$ and $6p_+$ states was neglected, giving the $\Psi(^1\Pi)$ the same separated-atom limit as the $\Psi(^1\Sigma)$ state from $H(1s)+Cs(6p)$. The four molecular wave functions and potential curves resulting from the application of the linear variation principle to $\Psi(^1\Sigma)$ and the single eigenfunction of $\Psi(^1\Pi)$ symmetry thus provide the basis for a reasonable representation of the low-energy collision processes (5) and (6). The potential curves are given in Fig. 2.

C. Coupling matrix elements

The coupling matrix elements in this adiabatic representation are the radial operator d/dR and the angular operator L_y. The angular coupling operator is easily evaluated analytically for these wave functions, while the d/dR matrix element evaluation requires a rather laborious mixed numerical analytic procedure. The coupling matrix elements for processes (3) and (4) are given in Fig. 3; those for processes (5) and (6) are given in Fig. 4. All of the computations required were carried out with the standard programs[13,14] at the University of Texas molecular physics group.

The sets of approximate wave functions and potential curves generated as described herein should be valid representations at the large internuclear separations $R \gtrsim 5a_0$ which dominate these collision processes. The relative positions of the levels at large internuclear separation (the energy differences and the matrix elements that appear in the cross-section computations) are probably accurate to within a few percent. The energy differences

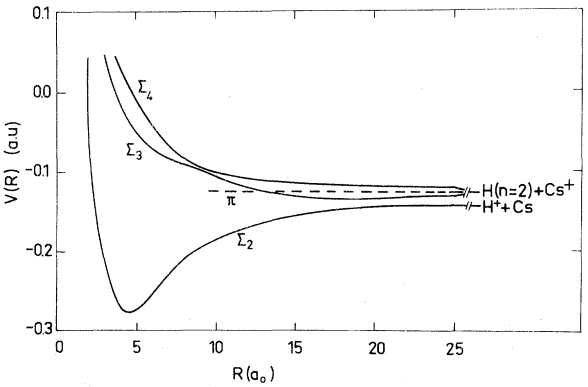

FIG. 1. CsH^+ one-electron *ab initio* potential-energy curves.

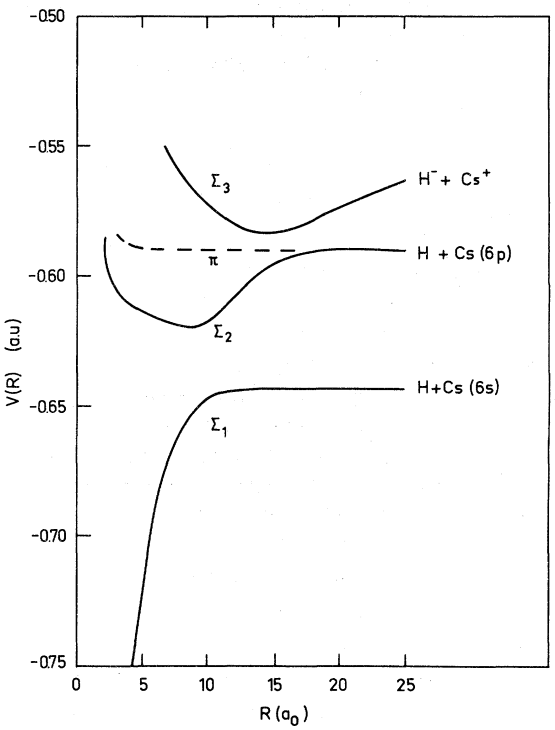

FIG. 2. CsH two-electron *ab initio* potential-energy curves.

were found to be virtually invariant to alterations in the wave-function basis. They will certainly become inaccurate rapidly at smaller internuclear separations. The absence of the Cs atomic ion will quickly cause the short-range potentials to be

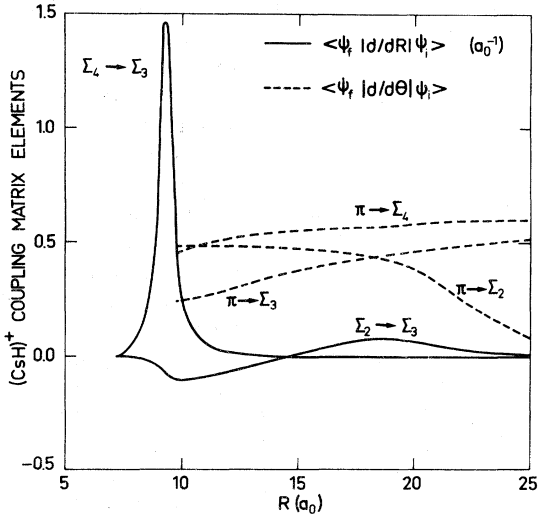

FIG. 3. CsH^+ radial $(\partial/\partial R)$ and rotational $(\partial/\partial\theta)$ coupling matrix elements.

less repulsive than the true short-range potentials. The potential curves and matrix elements computed herein agree qualitatively with those of Valance and Spiess[9] where comparison is possible.

III. CROSS SECTIONS

A. $H^+ + Cs$ and $H^- + Cs^+$ reactions

The cross-section calculations for reactions (3–6) were performed by solving the standard coupled equations where it is assumed that the nuclei follow classical trajectories. The equations were given by [15]

$$\frac{dC_i(Z)}{dZ} = -\sum_j \Gamma_{ij}(Z)\exp[-iW_{ij}(Z)]\,C_j(Z)\,, \quad (15)$$

where Z is related to the impact parameter b and internuclear separation R in the straight-line trajectory approximation by

$$Z^2 = R^2 - b^2\,. \quad (16)$$

The straight-line trajectory approximation is valid for these applications since the collision energies are much larger than the potential energies for the impact parameters that dominate the cross-section evaluation. The interaction potentials arise in Eq. (15) as differences via

$$W_{ij} = \frac{1}{\hbar v}\int_{-\infty}^{z}(V_j - V_i)\,dZ'\,, \quad (17)$$

while the coupling maxtrix elements are given by

$$\Gamma_{ij} = (Z/R)\langle\Psi_j|\partial/\partial R|\Psi_i\rangle + (b/R^2)\langle\Psi_j|\partial/\partial\Theta|\Psi_i\rangle\,. \quad (18)$$

The first term on the right-hand side of Eq. (18) corresponds to radial coupling, while the second term corresponds to rotational coupling. To obtain the cross section for a given transition to channel j, Eq. (15) is solved for a grid of impact parameters (normally $\Delta b = 0.25a_0$ was adequate), and the cross section is evaluated by the integral

$$Q_j = 2\pi\int_{b=0}^{\infty} db\, b\, C_j\,. \quad (19)$$

For impact parameters $b \leq 5a_0$, we continued to employ the one- and two-electron potential energies and coupling matrix elements in the cross-section calculations rather than to exclude these impact parameters from the evaluation. As an indication of their importance, the contribution to the cross sections by impact parameters $b \leq 5a_0$ was $\lesssim 10\%$ for Q_{+0}, Q_{+m}, and Q_{-0}, while it increased to $\lesssim 25\%$ for Q_{0-}.

To determine the cross sections for reactions (3) and (4), the CsH^+ potential-energy curves and coupling matrix elements, Figs. 1 and 3, were substituted into Eqs. (15)–(19). For reactions (5) and (6), the same procedure was used except that the CsH potential energies and coupling matrix elements, Figs. 2 and 4, were employed.

The results of the $H^+ + Cs$ calculations to obtain Q_{+0}, reaction (3), are displayed in Fig. 5. The calculated cross section has a broad maximum around 500 eV with a magnitude of 1.25×10^{-14} cm^2 and decreases rapidly for energies less than 250 eV to a value of 3.5×10^{-15} cm^2 at 50 eV. At energies above 500 eV, the cross section decreases monotonically. The calculated cross section is found to be in good agreement with recent experimental values.[16–19] The theoretical cross section tends to lie somewhat above the experimental values. A very probable reason for this difference is that we have not included excitation to $H^+ + Cs(6p)$, which proceeds via a curve crossing at $R \approx 9a_0$ with the Σ_4 state shown in Fig. 1. From the close-coupled calculations, we can make a rough estimate of the cross section for direct excitation of Cs and find $Q \lesssim 2\times10^{-15}$ cm^2. Thus, it is very possible that the theoretical cross sections are overestimated by (10–20)%. We should mention, however, that the absolute values of the experimental cross

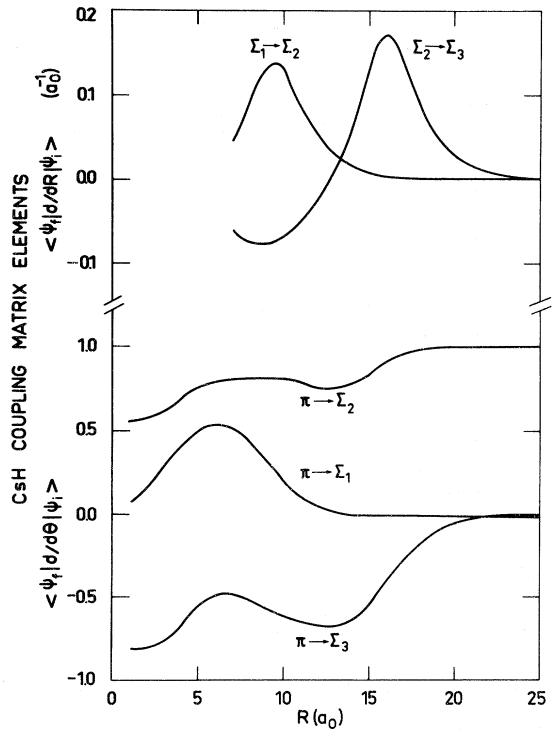

FIG. 4. CsH radial ($\partial/\partial R$) and rotational ($\partial/\partial\theta$) coupling matrix elements.

sections are accurate to (10–20)%, so even at present, theory and experiment are in agreement with one another.

The results of the Q_{+m} calculation, reaction (4), are a by-product of the $H^+ + Cs$ computations, and are also shown in Fig. 5. Here, we obtain a maximum value of 5.5×10^{-15} cm^2 at 500 eV, with the cross section decreasing to 1.7×10^{-15} cm^2 at 50 eV. At the higher energies, again the cross section is found to decrease monotonically. Comparing to the experimental data[3,20,21] that generally have error limits of ±30%,[3] it appears that the calculated Q_{+m} cross section is too large at the higher velocities. This same tendency occurred in the calculations of Valance and Spiess,[9] who only considered the radial coupling between the Σ states. Here, we have improved upon these previous calculations to include the rotational coupling to the $H(2p)+Cs^+$ productions, which effectively reduces the $H(2s)+Cs^+$ component, Q_{+m}, of the over-all charge-exchange cross section, Q_{+0}. Thus, we have no ready explanation for the discrepancy at the higher energies.

The ion-ion mutual neutralization cross section Q_{-0} for reaction (5), and the cross section for the reverse reaction, Q_{0-}, from ground-state reactants were computed using the CsH potential-energy curves and matrix elements, Figs. 2 and 4, in the classical coupled formalism, Eqs. (15)–(19).

The calculated Q_{-0} cross section is displayed in Fig. 6. Unfortunately, there are no experimental data to compare to the theoretical values. From the calculations, the major products formed, over 90%, are $H+Cs(6p)$. One might argue that the inclusion of higher-lying excited states of $H+Cs^*$ might further increase the Q_{-0} cross section. However, semiempirical calculations of the potential-energy splittings at these curve crossings,[22] backed up by Rydberg-Klein-Rees (RKR) studies[23] on the $H+Cs(6d)$ state, indicate that the splittings will be too small to greatly increase the cross section at the high energies. At lower energies, however, the higher-lying states will become increasingly important and must be included in any serious calculation.

The electron-transfer cross section, Q_{0-}, for formation of H^-+Cs^+ from ground-state reactants was also calculated. Here, it is possible to compare to the experimental data of Schlachter *et al.*[16] and Spiess et al.,[6] Fig. 6. The agreement is not encouraging. Since at these energies the inelastic cross section for a given system is only a function of relative velocity, measurements[16] of Q_{0-} for

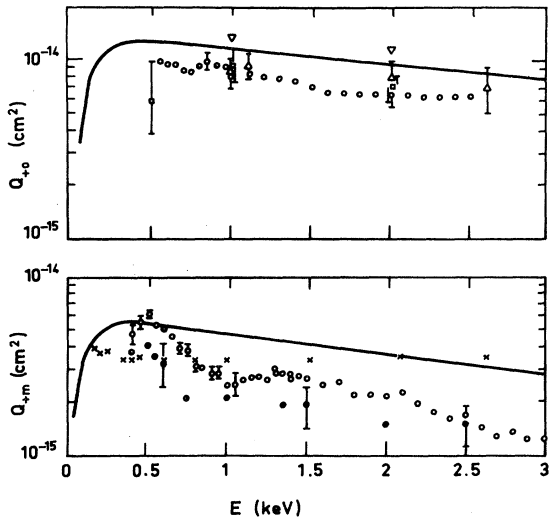

FIG. 5. The Q_{+0} cross section for reaction (3) and the Q_{+m} cross section for reaction (4). For Q_{+0}, the solid line represents the theoretical calculations, the open circles are the data of Spiess *et al.* (Ref. 18), the open squares are the data of Schlachter *et al.* (Ref. 16), the open triangles with error bars are the data of Grüebler *et al.* (Ref. 17), and the inverted open triangles are the recent data of Anderson and Meyer (Ref. 19). For the Q_{+m} graph, the solid line represents the theoretical calculations, the open circles are the data of Pradel *et al.* (Ref. 3), the crosses are the data of Donnally *et al.* (Ref. 20), and the solid circles are the data of Taun *et al.* (Ref. 21).

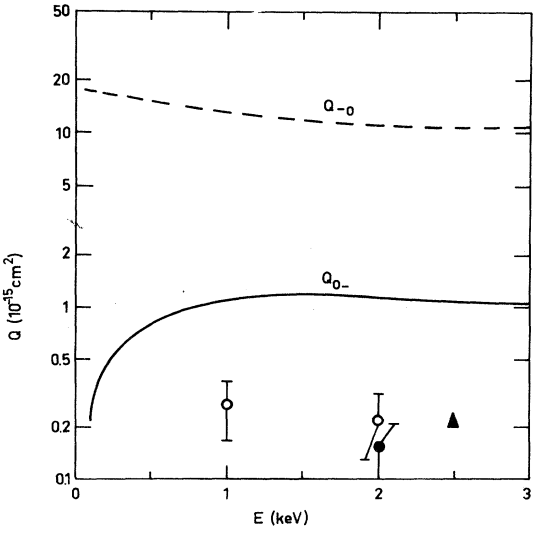

FIG. 6. Calculated Q_{-0} cross section (dashed line) for reaction (5) and the Q_{0-} cross section (solid line) for reaction (6). The solid triangle is the Q_{0-} cross section measured by Spiess *et al.* (Ref. 6), while the circles are the Q_{0-} cross sections measured by Schlachter *et al.* (Ref. 16). The solid circle is a H+Cs data point, while the open circles are D+Cs data that have been plotted on the H+Cs energy scale at half their collision energy.

D+Cs reactants are also displayed in Fig. 6. This makes it possible to compare the 4-keV D+Cs measurement to the 2-keV H+Cs measurement conducted on the same scattering apparatus. An interesting aspect of this comparison is that at 2-keV H+Cs relative energy, the D+Cs measurement for Q_{0-} is approximately 50% larger than the H+Cs measurement. This discrepancy was pointed out in Ref. 16, but no explanation was given. A very probable reason, however, is that a significant amount of the H^- and D^- is scattered outside the detection angle of the apparatus and is not counted. Reaction (6) would have considerable large-angle inelastic scattering because of the relative short-range nature of the interaction, giving rise to large-angle scattering off the repulsive walls of the potentials combined with the long-range Coulomb exit potential which also contributes to the large-angle scattering. Moreover, since the inelastic scattering for a given system is a function of energy times angle,[24] $E\theta$, we would expect at a given relative velocity that the large-angle-scattering correction for D+Cs would be much less than for H+Cs. Hence, if there is this problem, the experimental value of Q_{0-} for D+Cs at a given relative velocity would be larger than Q_{0-} for H+Cs. Since this is the observation, we tend to conclude that the experimental cross sections are affected by the large-angle scattering and tend to be too small. Whether this explanation can explain the large discrepancy between theory and experiment will have to await further investigation.

B. H^- + Cs ionization

The calculation of the ionization cross sections for reactions (7) and (8) is based on a mechanism used to explain some $He(2\,^3S)+He \rightarrow He^+ + He + e$ differential cross sections.[5] Here, it was shown that the diabatic potential of $He(2\,^3S)+He$ crossed directly into the $He_2^+ + e$ continuum. It was observed that the particles preferentially lost a low-energy electron at or near the curve crossing to the continuum.

The same arguments can be used for the H^-+Cs ionization reaction. A schematic diagram of the reaction is shown in Fig. 7. The H^-+Cs particles are assumed to follow the diabatic potential curve that crosses into the continuum where the electron is ejected. Since the curve crossing is estimated to be located at $7.0a_0$, the total ionization cross section will be πR_x^2, or 4.3×10^{-15} cm^2.

However, since we now have the CsH potential-energy curves (Fig. 2), it is possible to estimate the products of the ionization reaction. The *ab initio* potential-energy splittings at the curve crossings along with the rotational coupling to the H+Cs(6*p*) can be incorporated into Landau-Zener calculations to calculate the prbability of transition at each curve crossing and to determine the products of the reaction. The results of the calculations are shown in Fig. 8. At low energies the particles are not able to transit the curve crossings, and H+Cs products are preferentially formed. However, as the collision energy is increased, the particles prefer to remain on the diabatic potential curve so H^-+Cs^+ products become increasingly important.

The calculated cross section, $Q_{\text{ion-H}}$, for the formation of neutral products, reaction (8), is given by the solid line in Fig. 8 and can be compared to the experimental data of Leslie *et al.*[25] and Spiess *et al.*[6] The agreement is satisfactory. There are no experimental data with which to compare the theoretical cross sections, $Q_{\text{ion-Cs}}$, for production of H^-+Cs^+. However, at collision

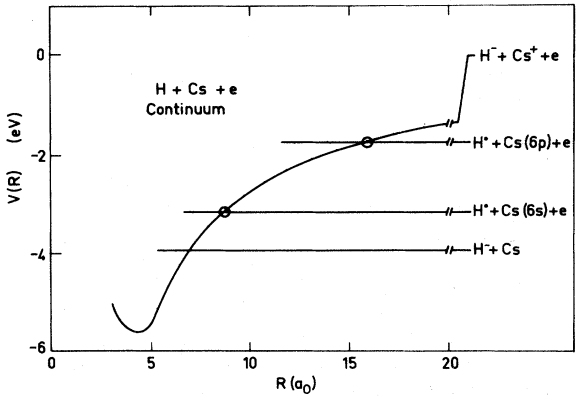

FIG. 7. Schematic diagram of the H^-+ Cs ionization processes.

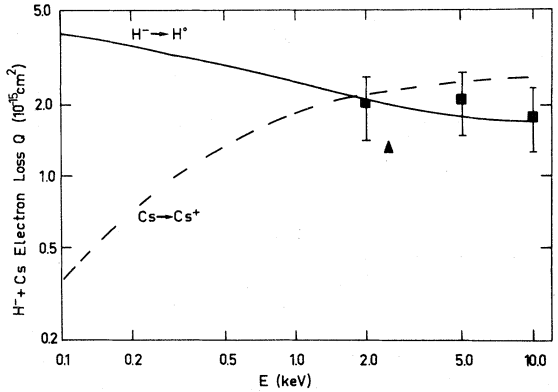

FIG. 8. H^-+ Cs ionization cross sections. The solid line is the calculated $Q_{\text{ion-H}}$ cross section for reaction (8), while the dashed line is the $Q_{\text{ion-Cs}}$ cross section for reaction (7). The solid triangle is the $Q_{\text{ion-H}}$ cross section measured by Spiess *et al.* (Ref. 6), while the solid squares are the $Q_{\text{ion-H}}$ cross sections measured by Leslie *et al.* (Ref. 25).

energies above 2 keV, the theoretical computations indicate that formation of $H^- + Cs^+ + e$ will be the dominant product of the $H^- + Cs$ ionization reaction.

C. H(2s) + Cs deactivation

The calculation of the deactivation cross section, Q_{mg}, for reaction (9) is based on previous work[8] where He and Ar, not Cs, were the targets in the collision with H(2s). The theory is semiempirical in nature because the potential-energy difference needed for the evaluation of the cross section is obtained from a parametrization given by Slocomb *et al.*[26] Furthermore, the assumption is made that, because of the near degeneracy at infinite internuclear separation between $H(2s) + X$ and $H(2p) + X$, the Q_{mg} cross section can be calculated in the same manner as for resonant scattering. This approximation is valid down to very low collision energies, approximately 0.1 eV, and is only compromised at the higher energies because additional deactivation channels invalidate the use of only two states. Within this framework the cross section is only a function of the velocity and the difference in potential energy between the Σ states arising from $H(n=2) + X$.

The potential-energy difference has been parametrized by Slocomb *et al.*,[26] using the potential calculations of Byron and Gersten,[27] to have the form

$$\Delta V(R) \sim 1020 \alpha_d R^{-7}, \tag{20}$$

where all quantities are in a.u. and α_d is the dipole polarizability of the target gas. Using Eq. (20), we may employ the Landau-Lifschitz approximation[28] to analytically obtain the deactivation cross section:

$$Q_{mg} = (5.3 \times 10^{-16}\ \text{cm}^2)(\alpha_d / v)^{1/3}. \tag{21}$$

In Eq. (21), α_d and the velocity v are in a.u.

To calculate the cross section for reaction (9), the dipole polarizability of Cs,[29] $363 a_0^3$, was substituted into Eq. (21). The results of the calculation are shown in Fig. 9 along with experimental estimates of this cross section.[7] The agreement is most encouraging considering that the error estimates of the experimental values are a factor of 2 and that from experience,[8] a similar error spread can be expected on the theoretical values obtained from Eq. (21).

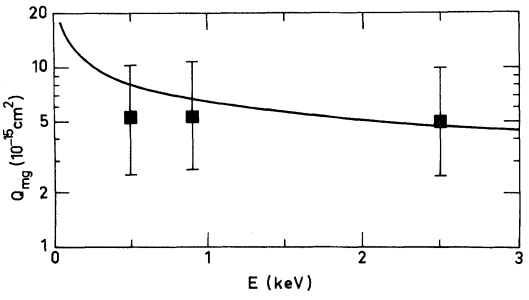

FIG. 9. The metastable H(2s) deactivation cross section Q_{mg} for reaction (9). The solid squares are Q_{mg} cross section estimates made by Schlachter (Ref. 7).

D. H(2s) + Cs negative ion formation

At present, the negative ion formation cross section Q_{m-} can only be estimated crudely by using the CsH potential-energy curves of Fig. 3. Since $H(2s) + Cs$ lies approximately 6.9 eV above the separated-atom limit of $H^- + Cs^+$, any interaction between these two states will be on the repulsive wall of the $H^- + Cs^+$ potential. An upper-limit cross section can then be calculated by πR_R^2, where R_R is an estimate of the repulsive wall dimension.

From Fig. 3, R_R can be estimated to be approximately $2a_0$, so $Q_{m-} \lesssim 4 \times 10^{-16}$ cm^2. Since the collision mechanism is expected to be a curve-crossing process, it is difficult to conclusively predict the energy dependence of the cross section. However, in general, one would expect since the interaction is on the repulsive wall of the potentials, that the cross section will be small at low collision energies and will increase with energy as the particles are more able to penetrate the repulsive barrier.

There has been no direct measurement of Q_{m-}. However, a value for Q_{m-} at 2.5 keV has been obtained by Pradel *et al.*[3] from an analysis of the H(2s) fractional yield under thick Cs target conditions for $H^+ + Cs$ collisions. The value is $\sim 5 \times 10^{-16}$ cm^2. Thus, there appears to be agreement between theory and experiment.

IV. CONCLUSIONS

This paper presents computed cross sections for and analyses of reactions between Cs and H atoms and ions that are important for the understanding of the collision processes occurring in polarized-ion sources. The primary stress here has been reactions proceeding at approximately 500 eV, since it is difficult to perform experiments at this low energy and because 500 eV is the nominal H collision energy used in the ion sources.

The cross sections were computed using a molecular basis set and coupling matrix elements obtained from *ab initio* calculations. Classical close-coupled equations were solved to obtain some of the cross sections. Other cross sections were obtained by semiempirical methods which are expected to be valid at these energies.

The agreement between theory and experiment is, in general, satisfactory, leading one to believe that the low-energy theoretical values are also satisfactory. The only serious discrepancy between theory and experiment is in the value for the Q_{0-} cross section. Since the theoretical cross section is very dependent on the potential-energy separation between the Σ_1 and Σ_2 potentials of CsH around $R \sim 9a_0$ (Fig. 3), we have rechecked our values by expanding the wave-function basis set used in the potential-energy calculations. The potential-energy separation was invariant to the wave-function charges; hence, we believe that the theoretical Q_{0-} cross section is reasonably accurate. Since experimental values are also in question, we believe that a more concentrated study, both theoretical and experimental, is due on reaction (6).

ACKNOWLEDGMENTS

One of the authors (R.E.O.) would like to thank Dr. Watel and Dr. Manus for the enjoyable opportunity to work in the Service De Physique Atomique at Centre d'Etudes Nucléaire, Saclay. The many stimulating discussions with Dr. Fred Schlachter are also appreciated.

---

*Senior Fulbright Fellow; present address: Molecular Physics Center, Stanford Research Institute, Menlo Park, Calif.

†Research supported by the Office of Naval Research under Contract No. N00014-67-A-0126-0017, and the Robert A. Welch Foundation of Houston, Texas.

[1]B. L. Donnally and W. Sawyer, Phys. Rev. Lett. 10, 439 (1965).
[2]L. D. Knutson, Phys. Rev. A 2, 1878 (1970).
[3]P. Pradel, F. Roussel, A. S. Schlachter, G. Spiess, and A. Valance, Phys. Rev. A 10, 797 (1974).
[4]R. E. Olson, Nucl. Instrum. Methods 126, 467 (1975).
[5]K. T. Gillen, D. C. Lorents, R. E. Olson, and J. R. Peterson, J. Phys. B 7, L327 (1974).
[6]G. Spiess, A. Valance, and P. Pradel, Phys. Lett. 31A, 434 (1970).
[7]A. Schlachter (private communication).
[8]V. Dose, W. Hett, R. E. Olson, P. Pradel, F. Roussel, A. S. Schlachter, and G. Spiess, Phys. Rev. A 12, 1261 (1975).
[9]A. Valance and G. Spiess, J. Chem. Phys. 63, 1487 (1975).
[10]H. Eyring, J. Walter, and G. E. Kimball, *Quantum Chemistry* (Wiley, New York, 1958).
[11]Reference 10, p. 162.
[12]J. N. Silverman, O. Platas, and F. A. Matsen, J. Chem. Phys. 32, 1042 (1962).
[13]F. A. Matsen and J. C. Browne, J. Phys. Chem. 66, 2332 (1962).
[14]J. C. Browne and F. A. Matsen, Phys. Rev. 135, A1227 (1964).
[15]D. R. Bates, H. S. Massey, and A. L. Stewart, Proc. R. Soc. Lond. A 216, 437 (1953).
[16]A. S. Schlachter, P. J. Bjorkholm, D. H. Loyd, L. W. Anderson, and A. Haeberli, Phys. Rev. 177, 184 (1969).
[17]W. Grüebler, P. A. Schmelzbach, V. König, and P. Marmier, Helv. Phys. Acta 43, 254 (1970).
[18]G. Spiess, A. Valance, and P. Pradel, Phys. Rev. A 6, 746 (1972).
[19]L. W. Anderson and F. W. Meyer, in *Electronic and Atomic Collisions, Abstracts of Papers of the Ninth International Conference on the Physics of Electronic and Atomic Collisions*, edited by J. S. Risley and R. Geballe (Washington U. P., 1975), p. 97.
[20]B. L. Donnally, T. Clapp, W. Sawyer, and M. Schultz, Phys. Rev. Lett. 12, 502 (1964).
[21]V. N. Taun, G. Gautherin, and A. S. Schlachter, Phys. Rev. A 9, 1242 (1974).
[22]R. E. Olson, F. T. Smith, and E. Bauer, Appl. Opt. 10, 1848 (1971).
[23]U. Ringstrom, J. Mol. Spectrosc. 36, 232 (1970).
[24]R. E. Olson and F. T. Smith, Phys. Rev. A 3, 1607 (1971).
[25]T. E. Leslie, K. P. Sarver, and L. W. Anderson, Phys. Rev. A 4, 403 (1971).
[26]C. A. Slocomb, W. H. Miller, and H. F. Schaeffer, J. Chem. Phys. 55, 926 (1971).
[27]F. W. Byron and J. I. Gersten, Phys. Rev. A 3, 620 (1971).
[28]R. B. Bernstein, in *Molecular Beams*, edited by J. Ross (Interscience, 1966), p. 118.
[29]A. Dalgarno and A. E. Kingston, Proc. Phys. Soc. Lond. 73, 455 (1959).